AIP | Journal of Applied Physics

Model for intermediate band solar cells incorporating carrier transport and recombination

Albert S. Lin, Weiming Wang, and Jamie D. Phillips

Citation: J. Appl. Phys. **105**, 064512 (2009); doi: 10.1063/1.3093962
View online: http://dx.doi.org/10.1063/1.3093962
View Table of Contents: http://jap.aip.org/resource/1/JAPIAU/v105/i6
Published by the American Institute of Physics.

Model for intermediate band solar cells incorporating carrier transport and recombination

Albert S. Lin,[a] Weiming Wang, and Jamie D. Phillips
Department of Electrical Engineering and Computer Science, Solid-State Electronics Laboratory, The University of Michigan, Ann Arbor, Michigan 48109-2122, USA

(Received 3 November 2008; accepted 3 February 2009; published online 24 March 2009)

A model for intermediate band solar cells is presented to assess the effect of carrier transport and recombination (CTR) on the efficiency of these devices. The model includes dependencies of physical parameters including optical absorption, carrier lifetime, and carrier transport on the density of intermediate band electronic states. Simulation results using this model indicate that conversion efficiency degrades when the net carrier recombination lifetime is small (range of nanoseconds) or when the device length is long relative to carrier drift length. The intermediate band solar cell model provides a method of determining realistic conversion efficiencies based on experimentally measurable input parameters for CTR. The incorporation of CTR provides insight on the dependence of optimal density of states and energetic position of the intermediate band based on carrier lifetime and mobility. The material ZnTeO (E_G=2.3 eV, E_I=1.8 eV) is used as a numerical example for the intermediate band solar cell model, where conversion efficiency drops from 30.36% to 19.4% for a 10 μm long device for a recombination lifetime decrease from 1 μs to 5 ns. The optimal impurity concentration is determined to be 10^{18} cm^{-3} for an optical absorption cross section of 10^{-14} cm^2. The conversion efficiency of a ZnTe solar cell with a total recombination lifetime of 10 ns is calculated to increase from 14.39% to 26.87% with the incorporation of oxygen. © *2009 American Institute of Physics*. [DOI: 10.1063/1.3093962]

I. INTRODUCTION

Single-junction photovoltaic solar cells have demonstrated the ability to achieve power conversion efficiency values near the maximum theoretical limit.[1,2] However, the maximum power conversion limitation for single-junction solar cells is lower than desired due to energy loss for solar photons with energy exceeding the bandgap energy and absence of solar cell response to solar photons with energy below the bandgap energy. Power conversion efficiency has been improved for tandem and multijunction solar cells, but these devices are more complex and are accompanied by higher manufacturing costs. In recent years, intermediate band solar cells (IBSCs) have been proposed to exceed efficiency limitations of conventional single-junction cells.[1,3] In these devices, electron states are introduced in the forbidden bandgap of a conventional semiconductor to provide three optical absorption bands to respond to incident solar energy. Previous calculations have suggested a theoretical 63.2% efficiency limitation[3] for single-junction IBSCs, motivating experimental efforts to realize these promising photovoltaic devices. Several approaches have been proposed to practically realize an IBSC, including quantum dots,[4–9] dopant impurities (often termed impurity-band photovoltaics),[10,11] and dilute semiconductor alloys.[12–21]

Since the original IBSC model by Luque and Martí in 1997,[3] there have been several continued efforts similar to this detailed balance approach.[22–31] Nevertheless, the effect of carrier transport and recombination (CTR) has not been adequately incorporated in these models despite the major impact of these processes on the solar cell conversion efficiency. The neglect of CTR in IBSC models ignores important physical characteristics of the devices, where proposed approaches of realizing an intermediate band (IB) are well known to strongly influence CTR properties in the material and ultimate solar cell conversion efficiency. The incorporation of impurities or introduction of a dilute alloy (e.g., N in III-N_x-V_{1-x} or O in II-O_x-VI_{1-x}) will significantly alter carrier transport and will typical decrease the minority carrier lifetime.[14,18,19,21] Techniques of synthesizing quantum dots may also increase nonradiative or interface recombination rates, while the radiative recombination lifetimes may be inherently short, in the range of nanoseconds.[21,32–36] It is therefore highly important to include the effects of CTR for IBSC models to ensure that calculated power conversion efficiency values are not significantly overestimated. The incorporation of CTR also provides a means of investigating the impact of important material parameters such as carrier mobility and minority carrier recombination lifetime on solar cell operation to properly guide the design and analysis of these devices. In this study, we assess the performance of IBSC via a semi-analytical model that incorporates the influence of finite carrier mobility and carrier recombination mechanisms to highlight the influence of these nonideal properties and their influence on conversion efficiency. The IBSC model presented is further applied to determine the optimal concentration of IB states and energetic position of these states for an IBSC.

[a]Electronic mail: shihchun@umich.edu.

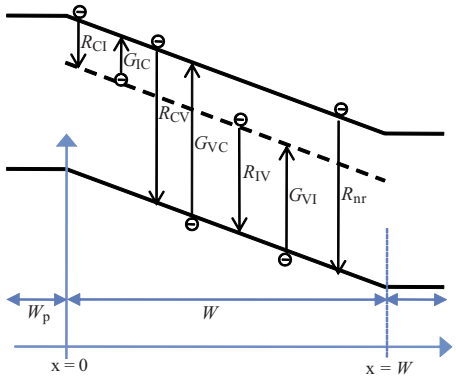

FIG. 1. (Color online) Illustration of device structure and generation-recombination mechanisms in the IBSC model.

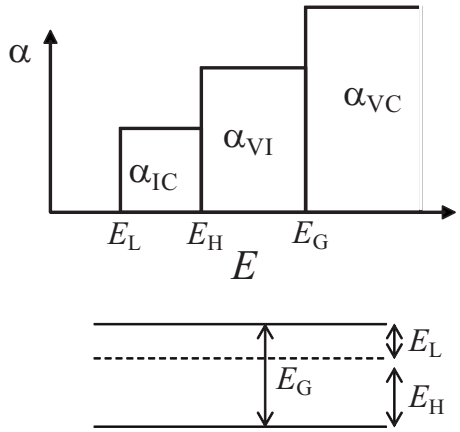

FIG. 2. Illustration of E_L, E_H, and E_G (top) and absorption coefficient vs photon energy (bottom).

II. MODEL DESCRIPTION

A common photovoltaic solar cell device structure proposed for the IBSC is the *p-i-n* (or *p-υ-n* and *p-π-n*) configuration,[4,5,7–9,37–39] which will also be used in this study (Fig. 1). This device structure incorporates a lightly doped absorber region and highly doped *p*- and *n*-type layers that clamp the built-in potential to maintain a large open circuit voltage.[37] The baseline photocurrent density due to valence band (VB) to conduction band (CB) optical transitions for this device structure may be expressed as[40–42]

$$J_{\text{ph,baseline}} = J_{L0}D[1 - \exp(-1/D)], \tag{1a}$$

$$D = l_c\left(1 - \frac{V_a}{V_{\text{bi}}}\right) \Big/ W, \tag{1b}$$

where W is the width of absorber, J_{L0} is the photocurrent density at large reverse bias,[41] μ_n and μ_p are the electron and hole mobilities, $\tau_{n,\text{tot}}$ and $\tau_{p,\text{tot}}$ are the total recombination lifetime values for electrons and holes, F is the electric field, l_n and l_p are the electron and hole drift lengths, and l_c is the collection length defined by $l_c = l_n + l_p = \mu_n F \tau_{n,\text{tot}} + \mu_p F \tau_{p,\text{tot}}$. The ratio of $W/[l_c(1 - V_a/V_{\text{bi}})]$ determines the charge collection efficiency, where the case of large W with respect to drift length would result in low charge collection efficiency due to carrier recombination prior to collection at the *p*- and *n*-type emitters.

The IB provides an additional generation-recombination path represented by

$$G_{\text{IC}}(x) = \int_{E_L}^{E_H} \alpha_{\text{IC}}(E) I_0(E) \exp[-\alpha_{\text{tot}}(E)x] dE, \tag{2a}$$

$$G_{\text{VI}}(x) = \int_{E_H}^{E_G} \alpha_{\text{VI}}(E) I_0(E) \exp[-\alpha_{\text{tot}}(E)x] dE, \tag{2b}$$

where G_{IC} is the generation rate from IB to CB and G_{VI} is the generation rate from valence to IB, $I_0(E)$ is the incident light from the solar spectrum, E represents energy, and α_{IC} and α_{VI} are the absorption coefficients for IB to CB and VB to IB transitions, respectively. The solar spectrum can be given as

$$I_0(E) = f_s X \frac{2\pi}{h^3 c^2} \frac{E^2}{\exp\left(\frac{E}{kT_{\text{sun}}}\right) - 1}, \tag{3}$$

where $f_s = 1/46\,050$ is the solid angle subtended by the sun, X is the solar concentration, $T_{\text{sun}} = 5963$ K is the temperature of the sun, k is the Boltzmann constant, c is the speed of light, and h is the Planck constant. In this study, $X = 1$ (one sun condition) is assumed unless otherwise noted. The absorption coefficient for the optical transitions is dependent on carrier occupation in the intermediate electronic states, represented by[6]

$$\alpha_{\text{IC}} = \alpha_{\text{IC0}} f, \quad \alpha_{\text{VI}} = \alpha_{\text{VI0}}(1 - f), \tag{4}$$

where α_{IC} and α_{VI} are the absorption coefficients for IB to CB and VB to IB transitions, respectively (Fig. 2) and f characterizes the filling of IB. This formulation accounts for the effect of IB electron state filling on the absorption process, where the presence of an electron (hole) is required for IB (VB) to CB (IB) transitions. The absorption coefficient constants α_{IC0} and α_{VI0} represent the oscillator strength of the transitions and density of states in the energy bands.

The net photocurrent density due to photogenerated carriers via the IB may then be calculated by substituting the generation rates above into the continuity equation for photogenerated excess carriers, as described in the following. The uniform field approximation is used,[40] assuming that the electric field does not significantly vary across the lightly doped or intrinsic region. The electric field may deviate from this assumption near the edge of the depletion region but is not expected to significantly alter charge collection. The diffusion current is assumed to be negligible for this device, where the *i* (*υ*, *π*) region will be fully depleted and the drift field will be responsible for electron-hole pair separation for photogenerated carriers. The continuity equation for excess electron concentration can then be written as

$$\upsilon_n \frac{d\Delta n(x)}{dx} + \frac{\Delta n(x)}{\tau_{n,\text{tot}}} = G_{\text{IC}}(x),$$
$$\text{boundary condition: } \Delta n(0) = 0, \tag{5}$$

where $\upsilon_n = \mu_n F$, $F = V_{\text{bi}}/W$, μ_n is electron mobility, V_{bi} is the

built-in potential, W is the absorber base width, and $\tau_{n,\mathrm{tot}}$ is the net recombination lifetime for electrons in the CB. The boundary condition for this device defines that the excess carrier concentration vanishes at the depletion region edge under short circuit conditions.[37,38,40] The net recombination lifetime, including nonradiative processes, may be described by

$$1/\tau_{n,\mathrm{tot}} = 1/\tau_{\mathrm{CI}} + 1/\tau_{\mathrm{CV}} + 1/\tau_{n,\mathrm{int}} + 1/\tau_{\mathrm{nr}}. \tag{6a}$$

Similarly for holes, the net recombination lifetime may be described by

$$1/\tau_{p,\mathrm{tot}} = 1/\tau_{\mathrm{IV}} + 1/\tau_{\mathrm{CV}} + 1/\tau_{p,\mathrm{int}} + 1/\tau_{\mathrm{nr}}, \tag{6b}$$

where τ_{CV}, τ_{CI}, and τ_{IV} are the radiative recombination lifetimes for CB to VB, CB to IB, and IB to VB transitions, respectively. The variable τ_{int} is the internal recombination lifetime, which represents recombination associated with the overlap between optical absorption spectra for the three transitions in the IBSC.[24] Nonradiative recombination is represented by the lifetime parameter τ_{nr}. The radiative carrier lifetimes associated with IB transitions, τ_{CI} and τ_{IV}, may be described as[25]

$$\tau_{\mathrm{CI}} = \left[\frac{1}{n_0}\frac{2\pi}{h^3c^2}\int_{E_L}^{E_H}\alpha_{\mathrm{IC}}\exp\left(-\frac{E}{kT}\right)E^2dE\right]^{-1}, \tag{7a}$$

$$\tau_{\mathrm{IV}} = \left[\frac{1}{p_0}\frac{2\pi}{h^3c^2}\int_{E_H}^{E_G}\alpha_{\mathrm{VI}}\exp\left(-\frac{E}{kT}\right)E^2dE\right]^{-1}, \tag{7b}$$

where n_0 and p_0 are the electron and hole equilibrium carrier concentrations. The energy values E_L, E_H, and E_G represent the edge of the absorption transitions, as shown in Fig. 2. The calculated values of τ_{CI} and τ_{IV} using Eqs. (7a) and (7b) are in the range of microseconds. Overlap between the absorption spectra of the optical transitions is assumed to be negligible in this analysis (neglect τ_{int}). Nonradiative recombination processes are lumped in the constant τ_{nr}, including Shockley–Read–Hall (SRH) and other nonradiative processes.

The solution to the continuity equation [Eq. (5)] is

$$\Delta n(x) = \int_0^x G_{\mathrm{IC}}(x')\exp\left(\frac{x'-W}{l_n}\right)dx', \tag{8}$$

where $l_n = v_n\tau_{n,\mathrm{tot}}$ is the electron drift length. The electron photocurrent density due to optical generation via the IB can then be determined by

$$J_{\mathrm{ph,IB},n} = qv_n\Delta n(W) = q\int_0^W G_{\mathrm{IC}}(x)\exp\left(\frac{x-W}{l_n}\right)dx. \tag{9a}$$

Similarly, the hole photocurrent density due to optical generation via the IB can be determined by

$$J_{\mathrm{ph,IB},p} = qv_p\Delta p(0) = q\int_0^W G_{\mathrm{VI}}(x)\exp\left(\frac{-x}{l_p}\right)dx. \tag{9b}$$

Substituting G_{IC} and G_{VI} [Eqs. (2a) and (2b)] into the electron and hole current density equations [Eqs. (9a) and (9b)], the IB occupation factor f may be solved by matching the electron and hole photocurrent densities,

$$J_{\mathrm{ph,IB},n}(f) = q\int G_{\mathrm{IC}}(x,f)\exp\left(\frac{x-W}{l_n}\right)dx = J_{\mathrm{ph,IB},p}(f) = q\int G_{\mathrm{VI}}(x,f)\exp\left(\frac{-x}{l_p}\right)dx. \tag{10}$$

The constraint to match the electron and hole photocurrent densities via the IB is based on the requirement that the net generation and recombination rate in the absorber are balanced to maintain charge neutrality. The IB occupation factor f may have a spatial dependence but is assumed to be a constant for the intrinsic or lightly doped absorber region.[3,23,24]

The diode dark current density may be expressed as

$$J_D = J_{\mathrm{diff}} + J_{\mathrm{r,CV}} + J_{\mathrm{r,CI}} + J_{\mathrm{nr}}. \tag{11a}$$

The first term J_{diff} is the diffusion current represented by

$$J_{\mathrm{diff}} = \left(\frac{qn_i^2D_n}{N_DW_p} + \frac{qn_i^2D_p}{N_AW_n}\right)\left[\exp\left(\frac{qV_a}{kT}\right) - 1\right], \tag{11b}$$

where V_a is the applied bias, W_p and W_n are the widths of the p- and n-type emitter layers, N_A and N_D are the acceptor and donor concentration in the p- and n-type emitter layers, n_i is the intrinsic carrier concentration, and D_n and D_p are the electron and hole diffusion coefficients. In this study, the device parameters for the heavily doped p- and n-type layers are assumed to be $W_p = W_n = 0.1$ μm and $N_A = N_D = 10^{19}$ cm^{-3}. The values of D_n and D_p are determined by the Einstein relation using the mobility values defined. The term $J_{\mathrm{r,CV}}$ is the radiative band to band recombination current density given by[3,22,23]

$$J_{\mathrm{r,CV}} = q\frac{2\pi}{h^3c^2}\int_{E_G}^{\infty} e^{-E/KT}E^2(1-e^{\alpha_{\mathrm{VC}}W})dE \times\left[\exp\left(\frac{qV_a}{kT}\right) - 1\right]. \tag{11c}$$

The radiative recombination current density due to the IB can be described by[3,22,23,26]

$$J_{\mathrm{r,CI}} = J_{0,\mathrm{r,CI}}\left[\exp\left(\frac{q\mu_{\mathrm{CI}}}{kT}\right) - 1\right] = J_{0,\mathrm{r,CI}}\left[\exp\left(\frac{qV_a(1-\xi)}{kT}\right) - 1\right], \tag{11d}$$

where $\mu_{\mathrm{CI}} = E_{\mathrm{FC}} - E_{\mathrm{FI}}$ represents the splitting of the Fermi level between CB and IB. The value of μ_{CI} is a fraction of V_a related by $(1-\xi)V_a$, where ξ is a value between 0 and 1 under dark conditions. The parameter ξ is determined by matching the electron and hole recombination current densities via the IB in the dark,

$$J_{\mathrm{r,CI}} = J_{0,\mathrm{r,CI}}\left[\exp\left(\frac{qV_a(1-\xi)}{kT}\right) - 1\right] = J_{0,\mathrm{r,IV}}\left[\exp\left(\frac{q\mu_{\mathrm{IV}}}{kT}\right) - 1\right] = J_{0,\mathrm{r,IV}}\left[\exp\left(\frac{qV_a\xi}{kT}\right) - 1\right] = J_{\mathrm{r,IV}}, \tag{11e}$$

where

$$J_{0,\mathrm{r,CI}} = q\frac{2\pi}{h^3c^2}\int_{E_L}^{E_H} e^{-E/KT}E^2(1-e^{\alpha_{\mathrm{IC}}W})dE, \tag{11f}$$

$$J_{0,\mathrm{r,IV}} = q\frac{2\pi}{h^3c^2}\int_{E_H}^{E_G} e^{-E/KT}E^2(1-e^{\alpha_{\mathrm{VI}}W})dE. \tag{11g}$$

The parameter $\mu_{\mathrm{IV}}=E_{\mathrm{FI}}-E_{\mathrm{FV}}$ can be represented as ξV_a due to the relation $\mu_{\mathrm{CI}}+\mu_{\mathrm{IV}}=(1-\xi)V_a+\xi V_a=V_a$.[3] The final term for nonradiative recombination current density J_{nr} can be given as

$$J_{\mathrm{nr}} = \frac{qn_iW}{2\tau_{\mathrm{tot}}\gamma}\left[\exp\left(\frac{qV_a}{2kT}\right)-1\right], \tag{11h}$$

where $\gamma=1+\tau_{\mathrm{nr}}/\tau_{\mathrm{r}}$. In this study, γ is generally assigned a value of 10 corresponding to a radiative efficiency of 90%, which is a typical value for a high quality direct bandgap semiconductor material such as GaAs. Finally, the total diode current density is determined by the sum of dark current and photocurrent due to VB to CB and IB radiative transitions,

$$J = J_D - (J_{\mathrm{ph,baseline}} + J_{\mathrm{ph,IB}}). \tag{12}$$

The power conversion efficiency of the solar cell is calculated as

$$\eta = \frac{J_{\mathrm{sc}}\times V_{\mathrm{oc}}\times \mathrm{FF}}{I_{\mathrm{sun}}}, \tag{13}$$

where J_{sc} is the short circuit current density, V_{oc} is the open circuit voltage, $\mathrm{FF}=J_mV_m/J_{\mathrm{sc}}V_{\mathrm{oc}}$ is the fill factor, and I_{sun} is the solar irradiance under one sun condition.[22] The values J_m and V_m are the current density and voltage at the operating point where the power output from the solar cell is maximum.

The model defined for IBSC devices in this work is applicable for any semiconductor material of interest. Material parameters for ZnTe are chosen in this analysis as a prototypical material for IBSC due to recent interest in oxygen-doped ZnTe as an active region for IBSC devices.[16,43] Two sets of device parameters are used in these simulations to investigate the influence of electron transport and carrier recombination: (1) $W=1$ μm with $\alpha_{\mathrm{IC0}}=\alpha_{\mathrm{VI0}}=10^3$ cm^{-1} and $\alpha_{\mathrm{VC}}=10^4$ cm^{-1} and (2) $W=10$ μm with $\alpha_{\mathrm{IC0}}=\alpha_{\mathrm{VI0}}=10^4$ cm^{-1} and $\alpha_{\mathrm{VC}}=10^4$ cm^{-1}. The parameters for device (1) represent the case of a realistic thin-film IBSC where the absorber region thickness is near 1 μm and the IB optical transition is an order of magnitude weaker than the VB to CB optical transition. The parameters for device (2) represent the case of a nearly ideal IBSC with a long absorption region and strong IB optical absorption. Detailed simulation parameters are indicated in the figure caption for each figure. The net electron and hole carrier lifetime values are assumed to be equivalent in these calculations for simplicity.

The physical processes associated with the IB will depend on the nature and density of the IB electronic states and will be material and process specific. As a first order approximation, the dependence of optical absorption and carrier lifetime will be related to the concentration of IB states (N_I) according to the following description. Optical absorption coefficients and net recombination lifetime are assumed to have the following linear relationships:[6,10,11]

$$\alpha_{\mathrm{IC}}(N_I) = \alpha_{\mathrm{IC0}}f = \sigma_{\mathrm{opt},n}N_If, \tag{14a}$$

$$\alpha_{\mathrm{VI}}(N_I) = \alpha_{\mathrm{VI0}}(1-f) = \sigma_{\mathrm{opt},p}N_I(1-f), \tag{14b}$$

$$\tau_{\mathrm{tot}}(N_{\mathrm{I}}) = \frac{1}{CN_I}, \tag{15}$$

where $\sigma_{\mathrm{opt},n}$ and $\sigma_{\mathrm{opt},p}$ are electron and hole optical absorption cross sections and C is the capture coefficient. The expressions in Eqs. (14a) and (14b) follow the formulation for SRH recombination and optical generation from localized donor or acceptor states[10,11] and has been recently used in the context of IBSC to explain experimental observations.[6] The recombination lifetime in Eq. (15) simply assumes that the recombination lifetime is inversely proportional to the concentration of IB states, similar to SRH lifetime where the lifetime is inversely proportional to trap density. The absorption coefficient α_{VC} and the prefactors α_{IC0} and α_{VI0} are defined in each simulation. Selected simulations define the optical absorption cross section, rather than α_{IC0} and α_{V0}, in order to study the effect of N_I on IBSC characteristics.

III. RESULTS AND DISCUSSION

The current-voltage characteristics for an IBSC with varying absorption coefficients for the IB are shown in Fig. 3(a), where the short circuit current density J_{sc} clearly increases with increasing α_{IC0} and α_{VI0} while the open circuit voltage V_{oc} does not change significantly. The increase in J_{sc} over the baseline cell (the case of $\alpha_{\mathrm{IC0}}=\alpha_{\mathrm{VI0}}=0$ cm^{-1}) is due to subbandgap photon absorption. The higher J_{sc} while maintaining nearly the same V_{oc} is the key aspect of IB photovoltaics. The slight decrease in V_{oc} in the case of $\alpha_{\mathrm{IC0}}=\alpha_{\mathrm{VI0}}=10^4$ cm^{-1} is due to the increase in radiative recombination current via the IB. The current-voltage characteristics calculated for the CTR model are compared to prior IBSC calculations that do not account for CTR, as shown in Fig. 3(b). Curves (1) and (2) are calculated using the model presented by Luque and Martí[3,24] while curve (3) is the result of the model presented here (CTR). Curve (1) is for an ideal IBSC with full absorption, fully concentrated sunlight, and infinite mobility. Curve (2) assumes a finite base width ($W=1$ μm) and no solar concentration ($X=1$). The material and device parameters (i.e., W, X, α, E_G, E_I) are the same for curves (2) and (3), where differences are the direct result of accounting for CTR. Differences in curves (2) and (3) from curve (1) are primarily related to the effect of assuming full absorption and fully concentrated sunlight. For curve (3), $V_{\mathrm{oc}}=1.80$ V and $J_{\mathrm{sc}}/X=18.30$ mA/cm^2 while for the ideal IBSC in curve (1), $V_{\mathrm{oc}}=2.28$ V and $J_{\mathrm{sc}}/X=30.88$ mA/cm^2. The reduced V_{oc} is primarily the result of assuming one sun condition ($X=1$) in comparison to fully concentrated sunlight assumed in previous studies.[3,24] Solar concentration effectively multiplies the short circuit current J_{sc} by the solar concentration factor X while also significantly increasing V_{oc}. The increase in V_{oc} is the result of increased generation rate, which in-

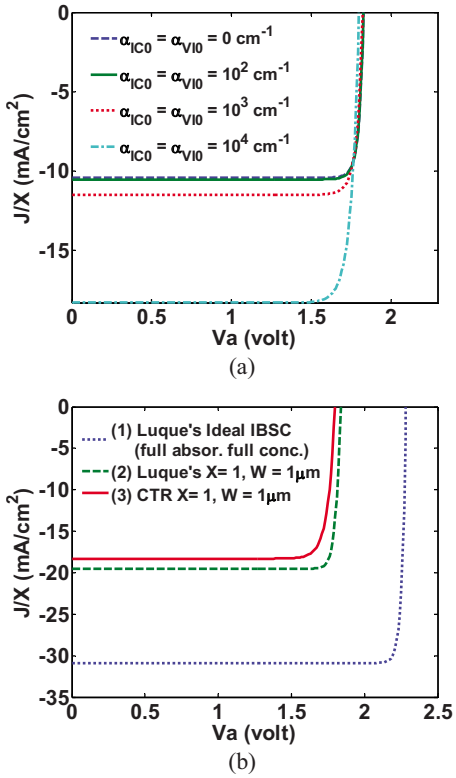

FIG. 3. (Color online) Current density vs voltage curves (a) comparing different absorption coefficients for IB transitions with $W=1$ μm, $\tau_{tot}=1$ μs, $\alpha_{VC}=10^4$ cm^{-1}, $E_G=2.3$ eV, $E_I=1.8$ eV, and $\mu_n=\mu_h=100$ cm^2/V s and (b) comparing the CTR model of this work to an ideal IBSC model (Ref. 3) with $\alpha_{VC}=10^4$ cm^{-1}, $\alpha_{IC0}=\alpha_{VI0}=10^4$ cm^{-1}, $E_G=2.3$ eV, and $E_I=1.8$ eV, and [for curve (3)] $\mu_n=\mu_h=100$ cm^2/V s and $\tau_{tot}=1$ μs.

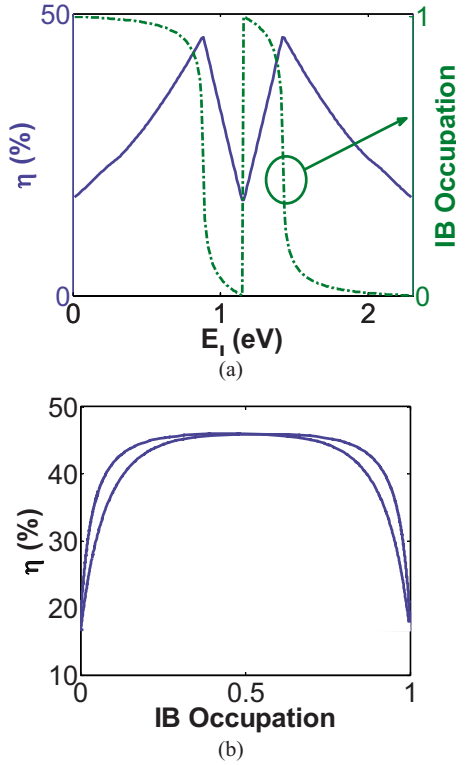

FIG. 4. (Color online) Efficiency dependence on IB characteristics as shown by (a) efficiency vs IB energy level (E_I) and (b) efficiency vs IB occupation.

creases the energy separation between the electron and hole quasi-Fermi levels. The smaller J_{sc}/X predicted in the CTR model is a result of finite device length and consequent incomplete absorption.

The energetic position of the IB will strongly influence the power conversion efficiency of the solar cell. Calculations of the efficiency versus energetic position of IB electronic states with respect to the VB edge (E_I) are shown in Fig. 4(a), along with the occupation of electronic states in the IB. The occupation of IB electronic states is determined by the balance between generation-recombination mechanisms and carrier transport in the CB and VB. The occupation of IB states will affect optical transitions via the IB and resulting IBSC efficiency. It is generally believed that a half-filled IB is optimal, though it has not been clear how the occupation of IB states affects the efficiency since occupation is not accounted for in previous IBSC device models.[3,22,24,25,32] In these simulations, optimal efficiency is confirmed to be near 50% occupation, as shown in Fig. 4(b). Two curves appear in Fig. 4(b), corresponding to two possible efficiency values for a given value of IB occupation depending on the position of E_I.

Carrier recombination lifetime has a major influence on conversion efficiency, where the mitigation of nonradiative processes is highly important. The dependence of IBSC conversion efficiency on minority carrier lifetime and IB position is depicted in Fig. 5. In the case of $\tau_{tot}=1$ μs, the calculated efficiency provides similar results to previous models for an IBSC,[24] where maximum efficiency occurs when E_I is symmetrically at one-third and two-thirds of E_G. A decrease in τ_{tot}, which may result from the incorporation of impurities or quantum dots, nonradiative recombination, or lower and more realistic values for carrier lifetime, leads to lower conversion efficiency. In addition to the decrease in conversion efficiency with lower carrier lifetime, the peak conversion efficiency occurs with E_I nearer the midgap for the case of $E_I<E_G/2$ or nearer the CB for the case of $E_I>E_G/2$. The shift of the peak conversion efficiency to different E_I values is a result of the optical absorption characteristic proportional to $\exp(-\alpha x)$ along the device. The overall collection efficiency will therefore be much higher for photogenerated holes than electrons for light incident from the p side of the diode due to the higher optical generation rate near the p side

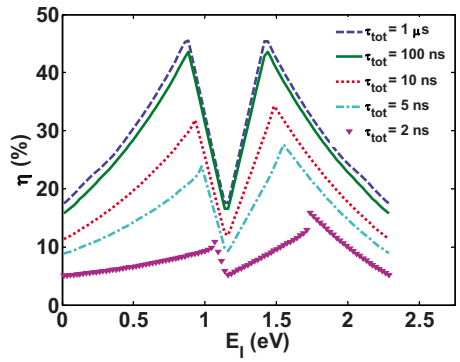

FIG. 5. (Color online) Efficiency vs IB energy level (E_I) for varying recombination lifetime values with $\alpha_{VC}=10^4$ cm^{-1}, $E_G=2.3$ eV, $\mu_n=\mu_h=100$ cm^2/V s, $W=10$ μm, and $\alpha_{IC0}=\alpha_{VI0}=10^4$ cm^{-1}.

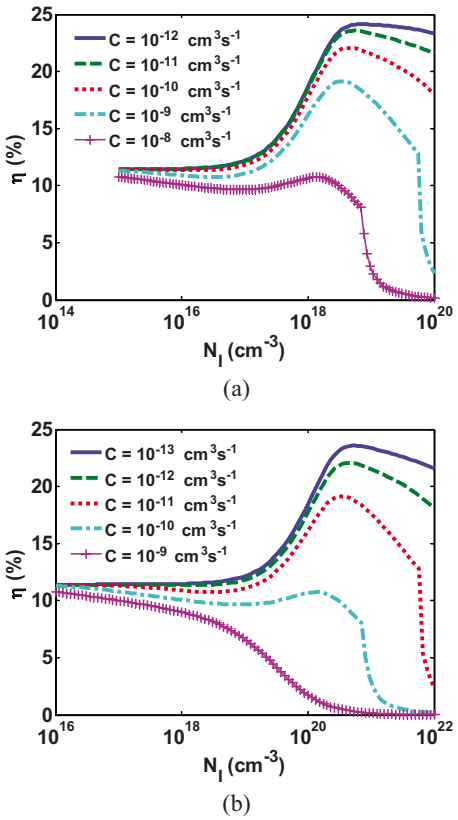

FIG. 6. (Color online) Efficiency vs density of IB states (N_I) for a device with a base width of $W=1$ μm, $\alpha_{VC}=10^4$ cm^{-1}, $E_G=2.3$ eV, $E_I=1.8$ eV, $\mu_n=\mu_h=100$ cm^2/V s, and $\alpha_{IC0}=\alpha_{VI0}=10^3$ cm^{-1} with values of optical cross section of (a) $\sigma_{opt}=10^{-14}$ cm^2 and (b) $\sigma_{opt}=10^{-16}$ cm^2.

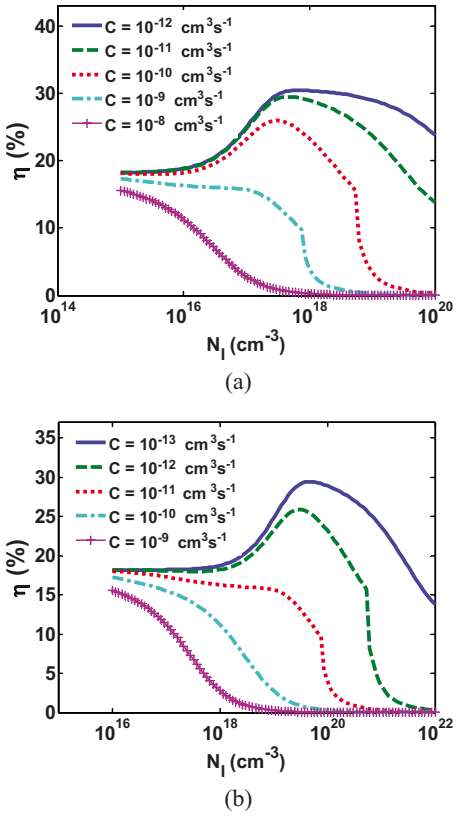

FIG. 7. (Color online) Efficiency vs density of IB states (N_I) for a device with a base width of $W=10$ μm, $\alpha_{VC}=10^4$ cm^{-1}, $E_G=2.3$ eV, $E_I=1.8$ eV, $\mu_n=\mu_h=100$ cm^2/V s, and $\alpha_{IC0}=\alpha_{VI0}=10^4$ cm^{-1}. (a) $\sigma_{opt}=10^{-14}$ cm^2. (b) $\sigma_{opt}=10^{-16}$ cm^2.

and shorter transport length for these excited holes. The maximum conversion efficiency will occur when the electron and hole photocurrents generated by the IB are both at a maximum.[3,24] Shorter carrier lifetime will result in more charge collection efficiency reduction in electrons than holes, and the shift in IB toward the CB edge will provide an increased absorption and corresponding photogeneration rate associated with the IB to CB transition to compensate for this. As a result, the peak efficiency will occur at an E_I value nearer the CB edge for shorter carrier lifetime. The optimal position for the IB will therefore have a dependence on the carrier lifetime value. It should be noted that the lifetime-dependent optimal position for E_I is a unique outcome of the CTR model employed in this work, a conclusion that is not found in previous models that neglect CTR.

The density of electronic states in the IB (N_I) will impact both optical absorption properties and carrier recombination processes. A quantitative understanding of these relationships is necessary for an accurate IBSC model. First order approximations of the influence of N_I on IBSC performance may be obtained by assuming values for optical absorption cross section and capture coefficient and evaluating trends with respect to conversion efficiency as described in Sec. II. Plots of calculated efficiency versus N_I are shown in Figs. 6 and 7 for varying values of carrier lifetime, absorber width, optical absorption cross section, and capture coefficient. For a given set of material parameters, an optimal value for N_I can be found.

Increasing the optical absorption cross section σ_{opt} shifts the optimal N_I to lower values due to increased optical absorption via the IB. Increasing capture coefficient C also results in a shift of the optimal N_I to lower values but also results in reduced conversion efficiency due to faster relaxation of photogenerated carriers. For higher carrier capture, such as the $C=10^{-8}$ cm^3 s^{-1} curve, the benefit of the IB is lost and the efficiency of the IBSC is reduced to a value below a single junction without an IB. Large values for capture coefficient C represent correspondingly small values in carrier lifetime. Experimental data for $\alpha(N_I)$ and $\tau_{tot}(N_I)$ may alternatively be used in these calculations and would provide a more accurate method of evaluating the optimal N_I for a specific material system proposed for IBSC. The determination of optimal N_I in this work is another unique outcome of the CTR model that has not been previously examined and can guide the future design of IBSC given the establishment of IB physical parameters.

The IBSC device structure under study will have a strong dependence on carrier transport, where photogenerated carriers in the depletion/lightly doped region will need to drift to the n and p contacts prior to recombination. The carrier mobility will therefore be a crucial parameter for this device. The dependence of conversion efficiency on carrier mobility for a ZnTeO IBSC is shown in Fig. 8. Solar cell conversion efficiency increases with mobility and then approaches the ideal case where mobility is high enough for perfect charge collection. In the case of a 10 μm thick ab-

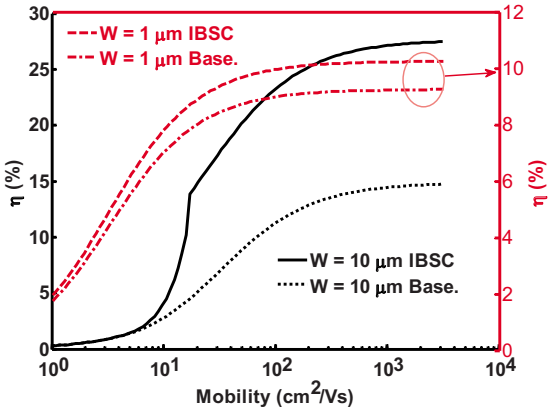

FIG. 8. (Color online) Efficiency vs carrier mobility comparing IBSCs with baseline solar cells without an IB. Material and device parameters are $\alpha_{VC}=10^4$ cm^{-1}, $E_G=2.3$ eV, and $E_I=1.8$ eV. For $W=1$ μm, $\alpha_{IC0}=\alpha_{VI0}=10^3$ cm^{-1} and $\tau_{tot}=1$ ns. For $W=10$ μm, $\alpha_{IC0}=\alpha_{VI0}=10^4$ cm^{-1} and $\tau_{tot}=10$ ns.

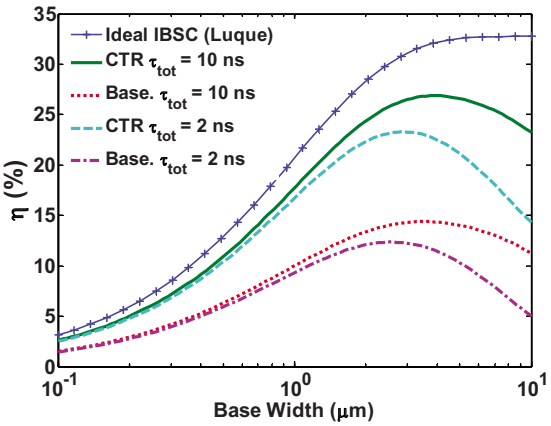

FIG. 10. (Color online) Efficiency vs base width comparing the CTR model of this work to an ideal IBSC solar cell and a baseline solar cell without an IB. Material and device parameters are $\alpha_{VC}=10^4$ cm^{-1}, $E_G=2.3$ eV, $E_I=1.8$ eV, and $\mu_n=\mu_h=100$ cm^2/V s, and $\alpha_{IC0}=\alpha_{VI0}=10^4$ cm^{-1}.

sorber region, the conversion efficiency can be much lower than the ideal case, where high mobility values would be necessary to ensure reasonable charge collection. This behavior implies the existence of an optimal base width, where shorter devices are beneficial in alleviating recombination loss while longer devices are preferred for higher optical absorbance.

The influence of charge collection on conversion efficiency is further illustrated by varying carrier lifetime, as shown in Fig. 9. The efficiency decreases significantly with carrier lifetime, where perfect charge collection does not occur for sufficiently thick absorption width and small recombination lifetime τ_{tot}. In a realistic IBSC device, it will be difficult to obtain both full optical absorption (long base width) and perfect charge collection (high carrier lifetime and mobility where the drift length is much longer than the base width). The CTR model presented provides a means of identifying and quantifying the optimal base width for an IBSC upon the establishment of physical material and device parameters.

The dependence of power conversion efficiency on base width for ZnTeO ($E_G=2.3$ eV, $E_I=1.8$ eV) is shown in Fig. 10 comparing an ideal IBSC (Luque and Martí's model[3] without CTR), a baseline ZnTe cell without IB using the CTR model, and a ZnTeO IBSC with IB using the CTR model. For the ideal IBSC, perfect charge collection is assumed, where the efficiency will increase with increasing base width W, saturating at a maximum efficiency for complete optical absorption at large W.[24] An optimal base width W is found for finite carrier mobility (CTR) associated with the trade-off between charge collection efficiency and optical absorption. The difference between the ideal IBSC model and CTR model becomes more pronounced at large base width where the effect of charge collection is no longer negligible. For the prototypical IBSC in this work, the optimal base width is in the range of $W\sim 2.9$ μm for $\tau_{tot}=2$ ns and $W\sim 3.9$ μm for $\tau_{tot}=10$ ns, as shown in Fig. 10. It should be noted that the presence of a backreflector and light trapping effect could reduce the optimal base width to about half of these values. The peak conversion efficiency for Luque and Martíı's model is 32.76%. The peak conversion efficiencies for IBSC using the CTR model are 26.87% and 23.29% when total recombination lifetimes are 10 and 2 ns, respectively, and the peak conversion efficiencies for the baseline cell are 14.39% for $\tau_{tot}=10$ ns and 12.34% for $\tau_{tot}=2$ ns.

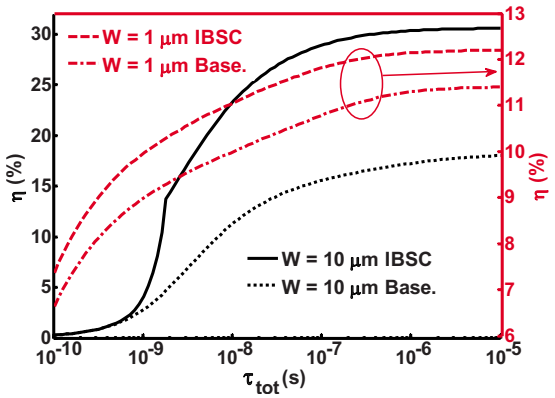

FIG. 9. (Color online) Efficiency vs total recombination lifetime comparing IBSCs with baseline solar cells without an IB. Material and device parameters are $\alpha_{VC}=10^4$ cm^{-1}, $E_G=2.3$ eV, $E_I=1.8$ eV, and $\mu_n=\mu_h=100$ cm^2/V s. For $W=1$ μm, $\alpha_{IC0}=\alpha_{VI0}=10^3$ cm^{-1}. For $W=10$ μm, $\alpha_{IC0}=\alpha_{VI0}=10^4$ cm^{-1}.

IV. CONCLUSION

A model is presented to assess the effect of charge transport and collection in IBSC based on electron and hole continuity equations and IB filling factor. Calculations using this model indicate that power conversion efficiency can be much smaller than the ideal case where infinite mobility and full absorption are assumed and provide quantitative data on the influence of these parameters. The design of IBSC devices is therefore facilitated by the CTR model, allowing one to determine optimal device parameters for a given IB material. The CTR model has also identified a lifetime-dependent optimal energetic position for the IB (E_I), which originates near $E_G/3$ from the band edge for large lifetime and shifts toward the CB edge with decreased carrier lifetime to compensate for carrier recombination. Similarly, the CTR has been used to identify the optimal density of IB states N_I associated with

the trade-off between optical absorption and carrier lifetime. The effect of carrier transport on solar cell efficiency was determined with varying parameters for mobility and carrier lifetime. The modeled dependence of conversion efficiency on carrier transport provides a means of determining the optimal base width W, provided with material parameters of the IB material (μ, τ_{tot}, α, E_G, E_I). ZnTeO is used as a prototypical IBSC example using the CTR model, where the peak conversion efficiency decreases from the theoretical, detailed balance limit value of 32.76% to 26.87% for a value of $\tau_{tot}=10$ ns in the CTR model and further decreases to 23.29% for $\tau_{tot}=2$ ns. Comparing the conversion efficiency at optimal base width, the improvement of a ZnTeO IBSC over a baseline cell without IB is an efficiency increase from 14.39% to 26.87% for $\tau_{tot}=10$ ns and from 12.34% to 23.29% for $\tau_{tot}=2$ ns.

[1] W. Schockley and H. J. Queisser, J. Appl. Phys. **32**, 510 (1961).
[2] M. A. Green, K. Emery, Y. Hishikawa, and W. Warta, Prog. Photovoltaics **16**, 435 (2008).
[3] A. Luque and A. Martí, Phys. Rev. Lett. **78**, 5014 (1997).
[4] C. D. Cress, S. M. Hubbard, B. J. Landi, R. P. Raffaellea, and D. M. Wilt, Appl. Phys. Lett. **91**, 183108 (2007).
[5] N. Usami, A. Amold, K. Fujiwara, K. Nakajima, T. Yokoyama, and Y. Shiraki, in Proceedings of the First IEEE International Conference on Group IV Photonics, Hong Kong, 2004 (unpublished), p. 130.
[6] A. Luque, J. Appl. Phys. **99**, 094503 (2006).
[7] R. Oshima, A. Takata, and Y. Okada, Appl. Phys. Lett. **93**, 083111 (2008).
[8] A. Alguno, N. Usami, T. Ujihara, K. Fujiwara, G. Sazaki, K. Nakajima, and Y. Shiraki, Appl. Phys. Lett. **83**, 1258 (2003).
[9] A. J. Nozik, Physica E **14**, 115 (2002).
[10] M. Schmeits and A. A. Mani, J. Appl. Phys. **85**, 2207 (1999).
[11] M. J. Keevers and M. A. Green, J. Appl. Phys. **75**, 4022 (1994).
[12] K. M. Y. W. Walukiewicz, J. Wu, J. W. Ager III, W. Shan, M. A. Scrapulla, O. D. Dubon, and P. Becla, in *Thin-Film Compound Semiconductor Photovoltaics*, MRS Symposia Proceedings, San Francisco, No. 865 (Materials Research Society, Warrendale, PA, 2005), p. F5.7.1.
[13] J. W. A. III, W. Walukiewicz, and K. M. Yu, "Ultrahigh efficiency multiband solar cells final report for director's innovation initiative project," LBNL Report No. 59768, 2006.
[14] S. Kurtz, S. W. Johnston, J. F. Geisz, D. J. Friedman, and A. J. Ptak, "Effect of nitrogen concentration on the performance of $Ga_{1-x}In_xN_yAs_{1-y}$ solar cells," NREL Report No. CP-520-37361, 2005.
[15] K. M. Yu, W. Walukiewicz, W. Shan, J. Wu, J. W. Beeman, M. A. Scarpulla, O. D. Dubon, and P. Becla, J. Appl. Phys. **95**, 6232 (2004).
[16] K. M. Yu, W. Walukiewicz, J. Wu, W. Shan, J. W. Beeman, M. A. Scarpulla, O. D. Dubon, and P. Becla, Phys. Rev. Lett. **91**, 246403 (2003).
[17] J. Wu, W. Shan, and W. Walukiewicz, Semicond. Sci. Technol. **17**, 860 (2002).
[18] O. Anton, D. Pate, C. S. Menoni, J.-Y. Yeh, L. Mawst, J. M. Pika, and N. Tansu, in Proceedings of the Conference on Lasers and Electro-Optics, San Francisco, CA, 2004 (unpublished), p. 16.
[19] S. Kurtz, J. F. Geisz, B. M. Keyes, W. K. Metzger, D. J. Friedman, J. M. Olson, A. J. Ptak, R. King, and N. H. Karam, Appl. Phys. Lett. **82**, 2634 (2003).
[20] K. M. Yu, W. Walukiewicz, J. W. Ager III, D. Bour, R. Farshchi, O. D. Dubon, S. X. Li, I. D. Sharp, and E. E. Haller, Appl. Phys. Lett. **88**, 092110 (2006).
[21] M. Smith, G. D. Chen, J. Y. Lin, H. X. Jiang, M. A. Khan, and Q. Chen, Appl. Phys. Lett. **69**, 2837 (1996).
[22] G. Wei, K.-T. Shiu, N. C. Giebink, and S. R. Forrest, Appl. Phys. Lett. **91**, 223507 (2007).
[23] A. Luque and A. Marti, Prog. Photovoltaics **9**, 73 (2001).
[24] T. S. Navruz and M. Saritas, Sol. Energy Mater. Sol. Cells **92**, 273 (2008).
[25] A. Martí, L. Cuadra, and A. Luque, IEEE Trans. Electron Devices **49**, 1632 (2002).
[26] L. Cuadra, A. Martí, and A. Luque, IEEE Trans. Electron Devices **51**, 1002 (2004).
[27] M. Ley, J. Boudaden, and Z. T. Kuznicki, J. Appl. Phys. **98**, 044905 (2005).
[28] A. S. Brown and M. A. Green, J. Appl. Phys. **94**, 6150 (2003).
[29] A. Luque, A. Martí, C. Stanley, N. López, L. Cuadra, D. Zhou, J. L. Pearson, and A. McKee, J. Appl. Phys. **96**, 903 (2004).
[30] A. Luque, A. Martí, and U. Cuadra, IEEE Trans. Electron Devices **48**(9), 2118 (2001).
[31] A. Luque, A. Martí, and L. Cuadra, IEEE Trans. Electron Devices **50**, 447 (2003).
[32] G. Wei and S. R. Forrest, Nano Lett. **7**, 218 (2007).
[33] K. Mukai, N. Ohtsuka, and M. Sugawara, Appl. Phys. Lett. **70**, 2416 (1997).
[34] M. Sugawara, K. Mukai, and H. Shoji, Appl. Phys. Lett. **71**, 2791 (1997).
[35] A. D. Andreev and E. P. O'Reilley, Appl. Phys. Lett. **79**, 521 (2001).
[36] S. Raymond, S. Fafard, P. J. Poole, A. Wojs, P. Hawrylak, S. Charbonneau, D. Leonard, R. Leon, P. M. Petroff, and J. L. Merz, Phys. Rev. B **54**, 11548 (1996).
[37] V. Aroutiounian, S. Petrosyan, A. Khachatryan, and K. Touryan, J. Appl. Phys. **89**, 2268 (2001).
[38] A. J. Nozik, "Quantum dot solar cells," NREL Report No. CP-590-31011, 2001.
[39] O. Jani, I. Ferguson, C. Honsberg, and S. Kurtz, Appl. Phys. Lett. **91**, 132117 (2007).
[40] R. S. Crandall, J. Appl. Phys. **54**, 7176 (1983).
[41] S. S. Hegedus, Prog. Photovoltaics **5**, 151 (1997).
[42] T. Markvart and L. Castaner, *Solar Cells: Materials, Manufacture and Operation* (Oxford: Elsevier Advanced Technology, Oxford, UK, 2005).
[43] W. Wang, A. Lin, and J. D. Phillips, J. Electron. Mater. **37**, 1044 (2008).